Climate Dynamics (2018) 51:2759–2772
https://doi.org/10.1007/s00382-017-4043-9

A process-level attribution of the annual cycle of surface temperature over the Maritime Continent

Yana Li[1] · Song Yang[1,2] · Yi Deng[3] · Xiaoming Hu[1,2] · Ming Cai[4]

Received: 2 February 2017 / Accepted: 5 December 2017 / Published online: 14 December 2017

Abstract
The annual cycle of the surface temperature over the Maritime Continent (MC) is characterized by two periods of rapid warming in March–April and September–October, respectively, and a period of rapid cooling in June–July. Based upon an analysis of energy balance within individual atmosphere–surface columns, the seasonal variations of surface temperature in the MC are partitioned into partial temperature changes associated with various radiative and non-radiative (dynamical) processes. The seasonal variations in direct solar forcing and surface latent heat flux show the largest positive contributions to the annual cycle of MC surface temperature while the changes in oceanic dynamics (including ocean heat content change) work against the temperature changes related to the annual cycle. The rapid warming in March–April is mainly a result of the changes in atmospheric quick processes and ocean–atmosphere coupling such as water vapor, surface latent heat flux, clouds, and atmospheric dynamics while the contributions from direct solar forcing and oceanic dynamics are negative. This feature is in contrast to that associated with the warming in September–October, which is driven mainly by the changes in solar forcing with a certain amount of contributions from water vapor and latent heat flux change. More contribution from atmospheric quick processes and ocean–atmosphere coupling in March–April coincides with the sudden northward movement of deep convection belt, while less contribution from these quick processes and coupling is accompanied with the convection belt slowly moving southward. The main contributors to the rapid cooling in June–July are the same as those to the rapid warming in March–April, and the cooling is also negatively contributed by direct solar forcing and oceanic dynamics. The changes in water vapor in all three periods contribute positively to the change in total temperature and they are associated with the change in the location of the center of large-scale moisture convergence during the onset and demise stages of the East Asian summer monsoon.

Keywords Maritime Continent · Annual cycle · Feedback attribution analysis

1 Introduction

The Maritime Continent (MC) is a main part of the Southeast Asian landmass and consists of the Malay Peninsula, Indonesia, Borneo, New Guinea and many other islands, and is situated between the Asian monsoon and the Australian summer monsoon region. As the main component of the "land bridge" (Lau and Chan 1983; Meehl 1987; Hung and Yanai 2004; Hung et al. 2004; Ding et al. 2014; Chang et al. 2016), the MC plays an essential role in regional and global climate variability. Previous studies have focused on the variations of deep convection over this region and its relationship with global climatic systems. For instance, (1) the Madden–Julian Oscillation (MJO) propagates across the MC in its mature phase and is modulated by the presence of MC. The convection associated with the active phase of the MJO

✉ Song Yang
yangsong3@mail.sysu.edu.cn

[1] School of Atmospheric Sciences, Sun Yat-sen University, 135 West Xingang Road, Guangzhou 510275, China

[2] Guangdong Province Key Laboratory for Climate Change and Natural Disaster Studies, Sun Yat-sen University, Guangzhou, China

[3] School of Earth and Atmospheric Sciences, Georgia Institute of Technology, Atlanta, GA, USA

[4] Department of Earth, Ocean, and Atmosphere Science, Florida State University, Tallahassee, FL, USA

becomes weakened and is split around the MC before it re-intensifies over the South Pacific convergence zone (Sui and Lau 1992; Zhu and Wang 1993; Chang 2004). (2) Deep convection strengthens and concentrated more over the southern MC during boreal winter, when the East Asian winter monsoon is stronger as more cold air mass from the interior of the Eurasian continent intrudes southward (Chang and Lau 1982; Lau and Chang 1987; Li and Yang 2010; Wang et al. 2010; Li and Yang 2017). (3) The rainfall over the MC tends to be negatively correlated with El Niño-Southern Oscillation: rainfall decreases during El Niño years and increases during La Niña years (Philander 1985; McBride et al. 2003; Hendon 2003; Chang et al. 2004; Wu et al. 2009; Wang et al. 2010; Cai et al. 2011). (4) Vividly described as a "boiled box" (Ramage 1968; Simpson et al. 1993), the deep convection over the MC serves as one of the main tropical energy sources (Neale and Slingo 2003). Exciting Rossby waves that propagate toward the extratropics, the strong convective heating over the MC exerts a significant impact on the winter circulation and surface temperatures across much of North America (Trenberth and Guillemot 1996; Yanai and Tomita 1998; Yang et al. 2002) and northeastern Eurasia (Neale and Slingo 2003).

The MC experiences a wet season in boreal winter and a dry season in boreal summer (Ramage 1968, 1971; Chang 2004), as the maximum convection marches gradually equatorward in boreal fall and northward in boreal spring (e.g., Lau and Chan 1983; Meehl 1987; Matsumoto 1992; Hung and Yanai 2004; Hung et al. 2004). The seasonal march and the overall intensity of precipitation are closely related with the land–sea distribution and complex terrain of the MC (Hung et al. 2004), and convective rainfalls are mostly concentrated over MC as a result of the land–sea breeze effect due to the land-sea thermal contrast (Qian 2008; Chang et al. 2016).

Compared with convective rainfalls, the temperature variation over MC receives much less attention despite it being an integral part of the regional energy and water cycle. However, the distribution of convective rainfall in the MC is closely tied to the distributions of MC land surface temperature and nearby sea surface temperature (SST) (Nicholls et al. 1996) because temperature anomaly is a footprint of sea level pressure anomaly causing anomalous convergence of wind, which is essential to deep convection. Therefore, these temperatures also play a fundamental role in shaping the patterns of general circulation over the western equatorial Pacific and beyond. Another well-known feature observed is that the seasonal march of convection over the MC is not symmetric: the maximum convection follows a gradually southeastward progression path from the Asian summer monsoon season to the winter monsoon season but experiences a sudden transition in the reverse (Schmidt and Ferguson 1951; Sukanto 1969; Hung et al. 2004; Chang 2004). This asymmetric transition has been suggested to the result of different land–ocean thermal memories during boreal spring and autumn, which has clear footprints in the surface temperature of the MC (van den Dool and Saha 1993; Chang et al. 2005a, b). In fact, most climate models even those with high resolutions show "dry" biases over the MC land, which are mostly due to inadequate representation of land-sea thermal contrast associated with the complex topography, leading to the systematic error in simulating the land-sea breeze in this region (Neale and Slingo 2003; Qian 2008). Webster and Yang (1992) pointed out that the spring prediction barrier of the SST over the western Pacific Ocean was a consequence of the rapid error growth over this region in spring time. All of these features suggest that it is necessary for us to understand better the variation of surface temperature over the MC and neighboring oceans and its drivers in order to achieve a better simulation and prediction of the regional climate.

As a first step, we start from the annual cycle of MC surface temperature and quantitatively estimate the contribution of each individual radiative and non-radiative (dynamical) process to the annual cycle of surface temperature in the context of the climate feedback-response analysis method (CFRAM). The details of the CFRAM method and the dataset used in this study are provided in Sect. 2. Section 3 describes the basic features of the surface temperature and its annual cycle in the MC region. Sections 4 and 5 present and discuss the main results including a process-level attribution of the temperature annual cycle and a close examination of the physical and dynamical processes responsible for the most rapid surface warming and cooling throughout a year. A summary is given in Sect. 6.

2 Data and method

The primary dataset used is the European Centre for Medium-range Weather Forecasts (ECMWF) Reanalysis Interim (ERA-Interim, Uppala et al. 2008; Dee et al. 2011). The data covers the period from 1979 to present with a horizontal resolution of 1° longitude × 1° latitude and 37 pressure levels in the vertical ranging from 1000 to 1 hPa.

The main analysis tool CFRAM is based on the total energy balance within an atmosphere–surface column at a given horizontal grid point that consists of M atmospheric layers and a surface layer (Cai and Lu 2009; Lu and Cai 2009a, b). Following Deng et al. (2012), we write the total energy balance equation separately for a month (i.e., February) and its preceding month (i.e., January), take the difference (Δ) between the 2 months (i.e., February–January), and obtain

$$\Delta\frac{\partial E}{\partial t} = \Delta S - \Delta R + \Delta Q^{non-radiative}, \quad (1)$$

where S(R) is the vertical profile of the net convergence (divergence) of short-wave (long-wave) radiation flux within

each layer. For all layers above the surface, $\Delta Q^{non\text{-}radiative}$ is the vertical profile of the convergence of total energy due to atmospheric turbulent, convective, and advective motions. At the surface, $\Delta Q^{non-radiative}$ corresponds to the loss of energy due to surface sensible and latent heat fluxes, as well as the net energy convergence in the ocean mixed layer if the surface is over oceans. The elements of $\frac{\partial E}{\partial t}$ represent the rate of energy storage change. All terms in Eq. (1) have units of W/m^2.

By omitting the high order terms of each thermodynamic feedback and the interactions among each thermodynamic feedback process, the total energy perturbation is obtained by adding linearly each process, commonly adopted by "climate feedback" works as Bony et al. (2006). Following Deng et al. (2013), we may express ΔS and ΔR as the sum of partial radiative energy flux convergence/divergence perturbations due to individual radiative feedback processes:

$$\Delta \mathrm{S} \approx \Delta S^{solar} + \Delta S^{wv} + \Delta S^{c} + \Delta S^{\alpha}$$
$$\text{and } \Delta \mathrm{R} \approx \Delta R^{wv} + \Delta R^{c} + \frac{\partial R}{\partial T}\Delta \mathrm{T}. \quad (2)$$

In Eq. (2), superscripts "solar", "wv", "c", and "α" denote solar insolation, water vapor, cloud, and surface albedo, respectively. Elements of ΔT are the vertical profile of temperature differences in each layer between months, and $\frac{\partial R}{\partial T}$ is the Planck feedback matrix whose *j*th column corresponds to the vertical profile of the radiative energy flux divergence perturbation due to 1 K warming at the *j*th layer from the preceding monthly temperature profile. Substituting Eq. (2) into Eq. (1), rearranging the terms and multiplying both sides of the resultant equation by $\left(\frac{\partial R}{\partial T}\right)^{-1}$, we obtain,

$$\Delta \mathrm{T} = \left(\frac{\partial R}{\partial T}\right)^{-1}\left\{\Delta S^{solar} + \Delta (S-R)^{wv} + \Delta (S-R)^{c} + \Delta S^{\alpha} + \Delta Q^{atmos\_dyn} + \Delta Q^{surface}\right\}. \quad (3)$$

The first four terms in Eq. (3) are ready to calculate since $\left(\frac{\partial R}{\partial T}\right)^{-1}$ and the partial radiative heating/cooling rate differences can be obtained by conducting off-line radiative transfer calculations. Variables required as input to the radiative transfer model (Fu and Liou 1992, 1993), including solar insolation at the top of the atmosphere (TOA), air/surface temperatures, specific humidity, cloud amount, cloud liquid/ice water content, surface albedo and ozone mixing ratio, are all obtained from the ERA-Interim. The quality of input data is examined by comparing the ERA-Interim with other reanalysis datasets such as the NCEP-NCAR Reanalysis II and the NASA MERRA2 (Modern-Era Retrospective analysis for Research and Application, Version 2) and observational references such as the NASA CERES (Cloud and the Earth's Radiant Energy System) and the OA Flux (Objectively Analyzed air–sea Fluxes) from the Woods Hole Oceanographic Institution (figures not shown). For the ERA-Interim data over the MC, net solar radiation and thermal radiation at surface are underestimated but better than those in the NCEP-NCAR Reanalysis II, compared with the CERES. Both surface latent and sensible heat fluxes are overestimated compared with the OA Flux. Based on the report of ECWMF and the work of Boilley and Wald (2015), the ERA-Interim also has non-negligible underestimation in cloud properties including cloud fraction, cloud ice water content, and cloud liquid water content, especially for lower clouds. Thus, the result of cloud contribution has been discussed with extra caution. Across the equatorial region over MC, ozone mixing ratio is larger in the thorough troposphere but smaller in the upper troposphere and the lower stratosphere, compared with the MERRA2. The qualities of other variables such as specific humidity, air/surface temperature, sea level pressure, and winds of the ERA-Interim are quite consistent with other reanalysis datasets. Therefore, in spite of these drawbacks discussed, regarding the long data record, high resolutions, and available variables, the ERA-Interim is of relative high quality for the present study.

ΔQ^{atmos_dyn} in Eq. (3) is zero at the surface layer, and in the atmosphere layers, $\Delta Q^{atmos\_dyn} = -\Delta(S-R)_{atmos}$, representing the vertical profile of the energy perturbation in the atmosphere associated with atmospheric motions (including turbulent, convective and large-scale motions) and heat storage anomalies (which is expected to be very small); $\Delta Q^{surface}$ is zero in atmosphere layers and at the surface layer, $\Delta Q^{surface} = -\Delta(S-R)_{surface}$, representing the energy perturbation at the surface due to surface turbulent sensible and latent heat flux anomalies, changes in the rate of heat storage (of the land or ocean), and oceanic circulations (if the surface is over ocean). Since the energy perturbations associated with surface turbulent heat fluxes $\left(\Delta Q^{lh} + \Delta Q^{sh}\right)$ can be obtained directly from the ERA Interim, we estimate the sum of the oceanic dynamics and land/ocean heat storage term as the residual of the surface energy balance equation, $\Delta Q^{ocean} = -\Delta(S-R)_{surface} - \left(\Delta Q^{lh} + \Delta Q^{sh}\right)$ (Sejas et al. 2014; Hu et al. 2016). It is noteworthy that ΔQ^{ocean} over lands is non-negligible when water sources are enough to affect the water cycle (i.e., over the MC). Equation (3) allows us to express the vertical profile of the temperature difference between 2 months in the atmosphere–surface column at a given horizontal location as the sum of the vertical profiles of the partial temperature changes (PTCs) due to changes in solar insolation, water vapor, cloud, surface albedo, atmospheric dynamical and surface dynamics/heat storage.

To quantify relative contributions of each individual processes to surface temperature anomalies over the MC both

in its spatial pattern and mean amplitude, we calculate the pattern-amplitude projection (PAP_i) using the partial temperature anomalies (ΔT_i) at surface associated with each individual process i. Following Park et al. (2012), we have

$$PAP_i = A^{-1}\int_A a^2 \Delta \mathrm{T}\cos\varphi \mathrm{d}\lambda \mathrm{d}\varphi \times \frac{A^{-1}\int_A a^2 \Delta T_i \Delta \mathrm{T}\cos\varphi \mathrm{d}\lambda \mathrm{d}\varphi}{A^{-1}\int_A a^2 (\Delta \mathrm{T})^2 \cos\varphi \mathrm{d}\lambda \mathrm{d}\varphi}, \quad (4)$$

where φ and λ are latitude and longitude, respectively, a is the mean radius of the earth, ΔT is the observed temperature anomalies and A represents the region, over which the spatial averaging is carried out and is the MC including its neighboring oceans in this case. By definition, the sum of PAP coefficients, just like the sum of PTCs averaged over the analysis region, equals the total temperature change averaged over the analysis region. The difference between an area averaged PTC and a PAP is that the latter emphasizes the "spatial similarity" between the PTC distribution and the total temperature change distribution and is therefore a better metric for assessing the overall contribution of a specific process to the temperature change over the region of consideration. Additionally, an extended PAP, the temporal pattern-amplitude projection ($TPAP$) method, is applied to quantify the relative contribution of each process annual variation to the annual cycle of observations,

$$TPAP_i = \frac{\sum_1^{12}\left(PAP_{in} * \Delta T_n\right)}{\sum_1^{12}\left(\Delta T_n\right)^2}, \quad (5)$$

where i and n refer to the ith feedback process and nth month from January to December, and ΔT is the observation. PAP and TPAP together give us an overall spatial and temporal projection to the observation.

3 Observed annual cycle of surface temperature in the Maritime Continent

Located in the warmest ocean around the globe, the surface temperatures in most parts of MC are above 300 K all year round (Fig. 1), while the month-to-month surface temperature variations still indicate a distinct seasonal cycle (Fig. 2). The northern portion (north of the equator) of the MC becomes warmer from February to May, and colder from June to January, while the southern portion (south of the equator) becomes warmer from August to November and from February to April, and colder from May to July and from December to January. Due to a smaller thermal inertia, the surface temperature over land changes more rapidly than that over the ocean, leading to a more pronounced annual cycle over the land. Considering the region as a whole, the MC is warmed from February to May and from September to November, and becomes cooled from June to August and from December to January, with the months of the fastest warming throughout a year in March–April and September–October, and the fastest cooling months in June–July.

The solar insolation is the most important forcing that drives the seasonal cycles in various atmospheric properties including temperature, precipitation and general circulation (Chen et al. 1994; Kodera and Kuroda 2002). To show the relationship between monthly-mean surface temperature and solar insolation at the TOA, we calculate the areal averages of both quantities over 10°S–10°N/90°–165°E. The climatology of the solar insolation and surface temperature is each characterized by two peaks in the annual cycle with the peaks of surface temperature lagging those of solar insolation by 1 or 2 months (Fig. 3a). The following analyses focus on the month-to-month temperature increments in the MC, which are shown in Fig. 3b. Consistent with the findings from Fig. 2, throughout a year, there are two largest positive increments, from March to April and from September to October, corresponding to the two periods of the most rapid warming. The temperature increment from June to July has the largest negative value, corresponding to the most rapid cooling. In the next two sections, we will attempt to attribute the temperature increments observed here into individual radiative and non-radiative (dynamical) processes.

4 Process-level attribution of the annual cycle of MC surface temperature

We first decompose the month-to-month increment in surface temperature into PTCs associated with various processes following the CFRAM method. The PAP coefficients (PAPs) [Eq. (4)] are then computed for each PTC to quantify the contribution of each process to the annual variation of surface temperature in the MC.

Based on the overall magnitudes of the PAPs shown in Fig. 4, the main contributors to the month-to-month temperature increments are the solar insolation at the TOA and the oceanic dynamics (including ocean heat storage change) (at approximately $\pm$5 K). Cloud and surface latent heat flux rank second at approximately $\pm$2 K, and water vapor, atmospheric dynamics and surface sensible heat flux contribute at the level of $\pm$0.6 K. The change in solar insolation has net positive contributions to the month-to-month temperature increment (indicated by the match of sign between the PAPs and the corresponding temperature increment) except for March–April, June–July and December–January (Fig. 4a). The PAPs associated with ocean dynamic/land–ocean heat storage (OCH) are negative from January to April and from August to October, and positive from May to June and from November to December (Fig. 4b). They are almost completely out of phase with the observed month-to-month

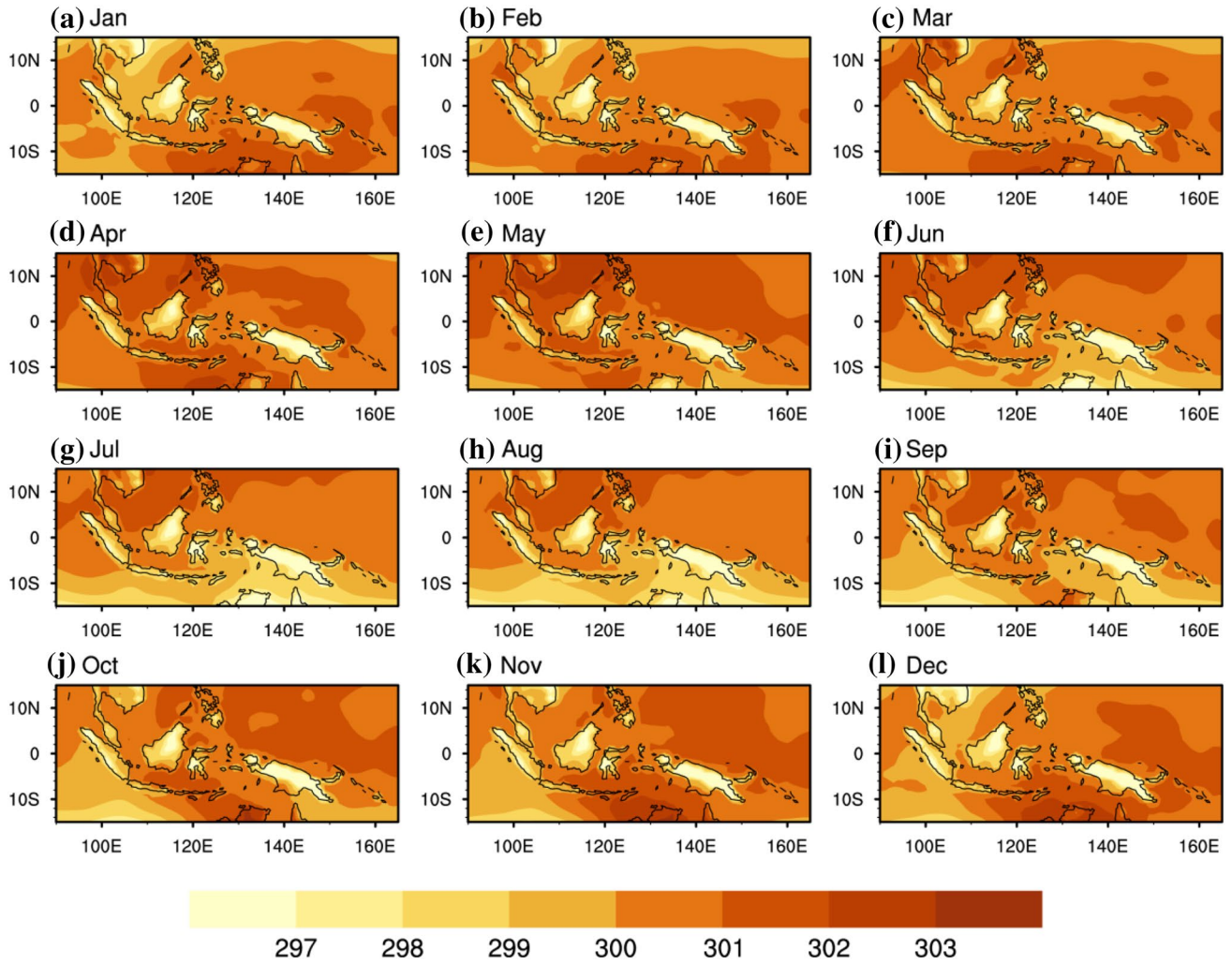

Fig. 1 Climatology of monthly mean near-surface temperature (T2m) during 1981–2010 (unit: K)

temperature increment (black solid curves in Fig. 4b), suggesting an overall negative contribution of oceanic dynamics to the seasonal variation of surface temperature in the MC. Given that the region of our focus is essentially the warm pool and that the surface (latent/sensible) heat flux is closely related with the heat condition of local oceans (Smith 1988), we may combine the effect of OCH with that of surface heat fluxes and treat this combination as the total effect of surface processes. The PAPs of the surface processes, given in Fig. 4c, are consistent with those of OCH (Fig. 4b), indicating a much greater amplitude of OCH in comparison to surface heat fluxes. In addition, the annual cycles of the PAPs associated with surface heat fluxes are nearly out of phase with those of OCH (Fig. 4g, b), suggesting that surface heat fluxes often work against OCH in producing surface temperature fluctuations. Water vapor, clouds, atmospheric dynamics, and surface latent heat fluxes all exhibit overall positive contributions to the month-to-month temperature increment in the MC region (Fig. 4d–g), with the magnitudes of the PAPs associated with clouds and surface latent fluxes being about two times greater than those associated with water vapor and atmospheric dynamics. In late summer and early fall (August–October), atmospheric dynamics and surface sensible heat fluxes have considerable negative contributions to the annual cycle.

To directly assess the overall contribution of each process to the annual cycle of surface temperature in the MC region, we further compute the *TPAP* following Eq. (5). For the entire MC region (10°S–10°N/90°–165°E), all radiative and non-radiative processes contribute positively to the annual cycle of surface temperature, except OCH (Fig. 5a). With large heat storage ability, the ocean acts as a buffer to store part of solar insolation that affects the surface temperature later, which is also shown in Fig. 4a as the PTCs of solar insolation lead observations by about 1or 2 months. As positive contributors, surface latent heat

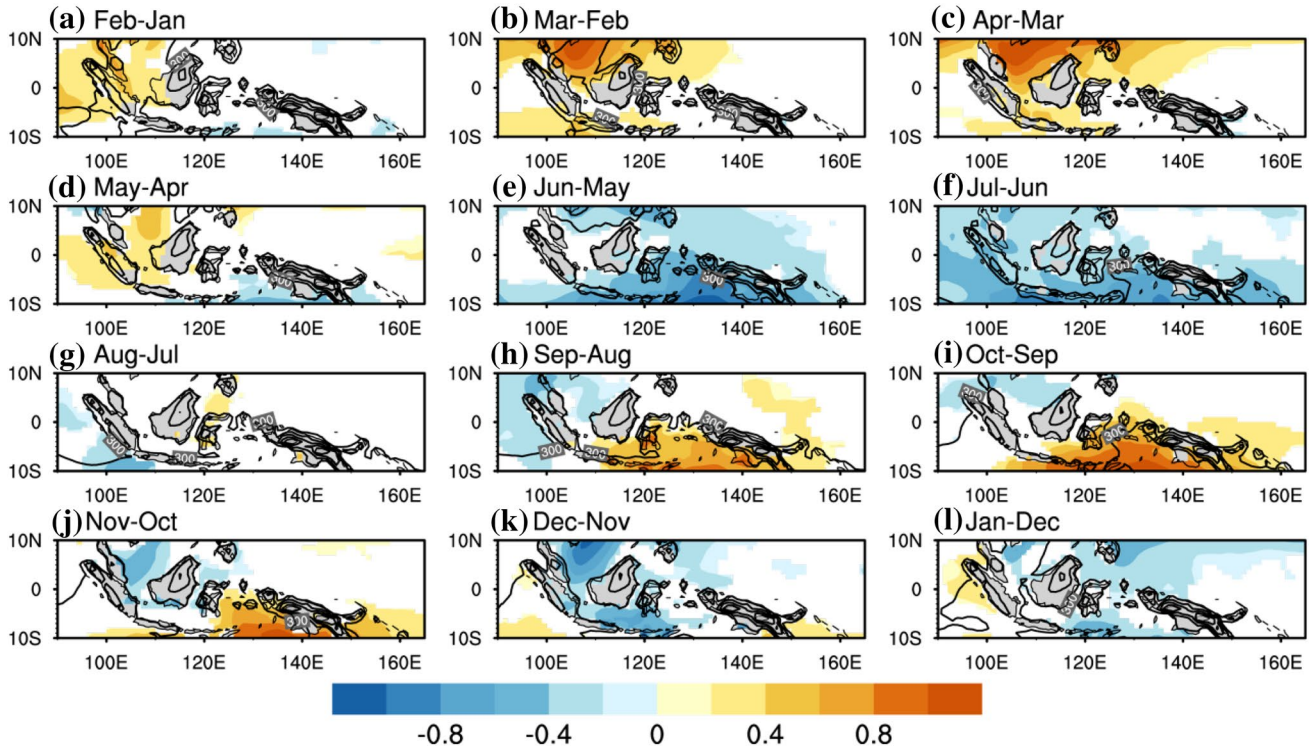

Fig. 2 Significant changes in surface temperature between contiguous months at 95% confidence level (shading, unit: K). Contours indicate the climatology of surface temperature in each month, for example, contours in (**a**) represent the climatology in January (contours, unit: K)

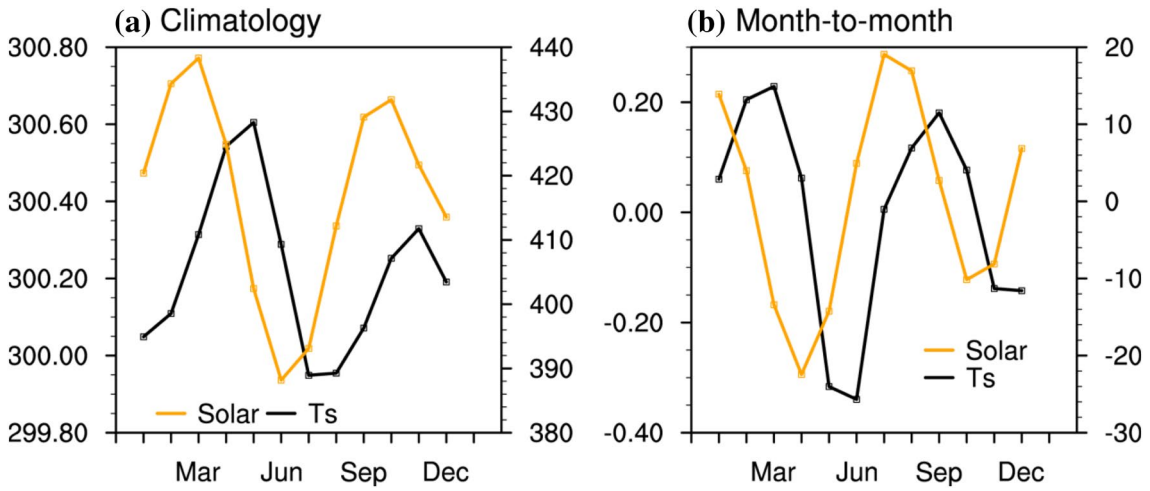

Fig. 3 **a** Climatology of annual variations of the solar radiation at the top of troposphere (TOA) (yellow solid line, corresponding to the right y-axis, unit: W/m^2) and surface temperature (black solid line, corresponding to the left y-axis, unit: K) average over 10°S–10°N/90°–165°E. **b** The increment between two months of solar radiation (yellow solid line) and surface temperature (black solid line), and the corresponding y-axis is same as in (**a**), for example, January represents the difference from January to February

flux and solar insolation contribute most to the surface temperature change over the northern and southern MC, respectively (Fig. 5b, c), and the contribution of solar insolation is more important to the southern MC than to the northern part. Since heat storage on land is negligible, the input of short-wave energy into the surface more directly manifests itself in the surface temperature over land. Thus, solar insolation is more important in the annual cycle of surface temperature to the southern MC, due mainly to the difference in land–ocean distributions as land/ocean ratio

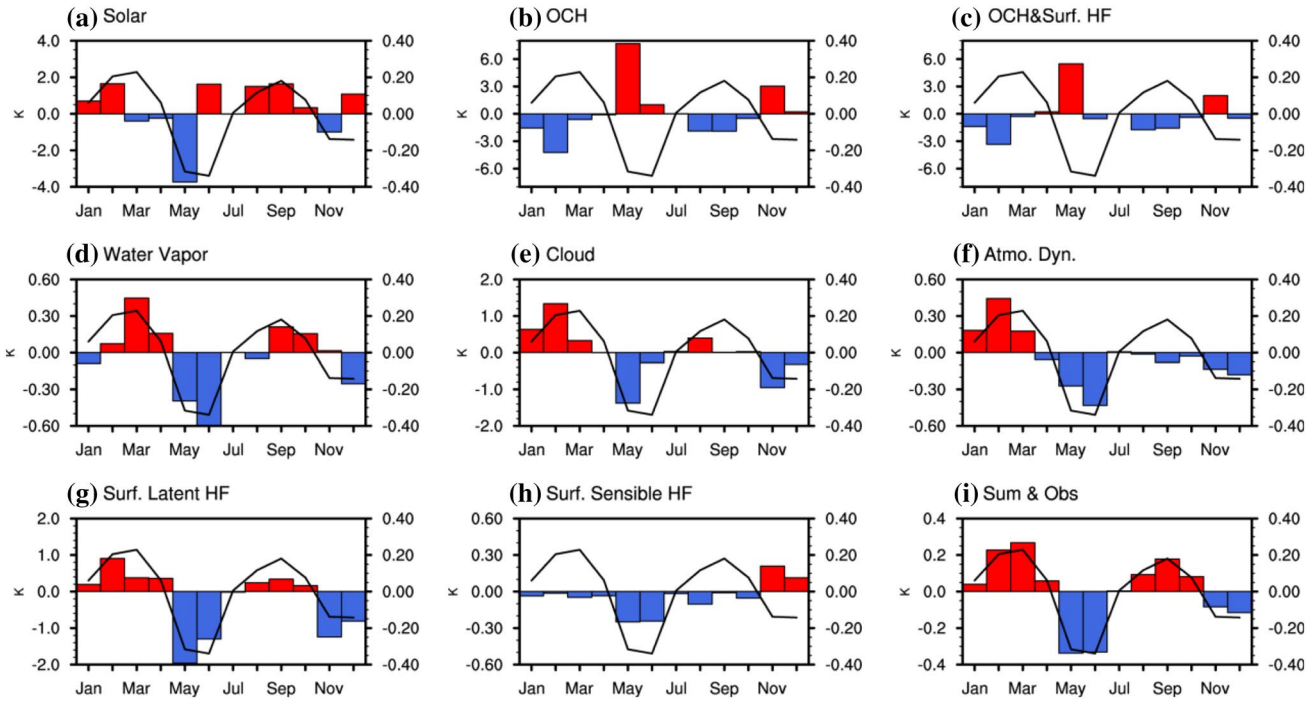

Fig. 4 Annual cycle of pattern-amplitude projection coefficients (PAPs) of surface temperature average over 10°S–10°N/90°–165°E due to changes in **a** solar radiation at the TOA, **b** oceanic dynamic and ocean/land heat storage (OCH), **c** OCH and surface heat flux, **d** water vapor, **e** cloud, **f** atmospheric dynamics, **g** surface latent heat flux, **h** surface sensible heat flux, and **i** sum of all individual feedback processes. The black solid lines in (**a**–**i**) refer to observations

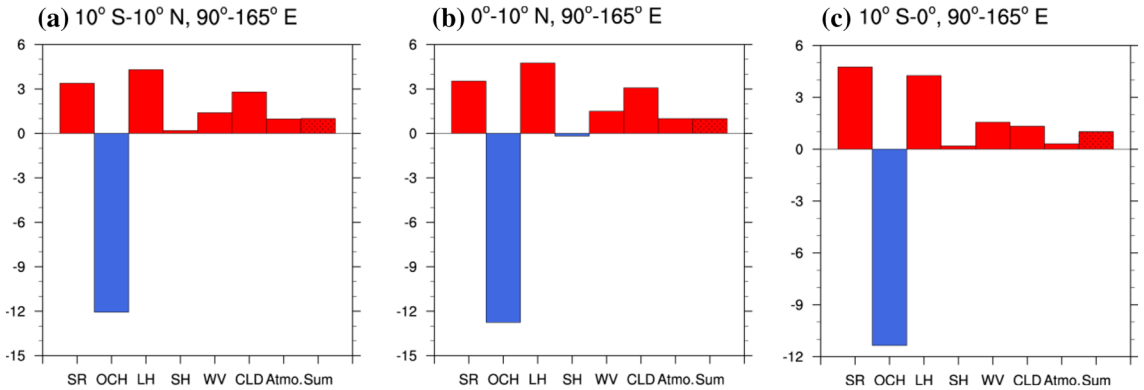

Fig. 5 Temporal pattern-amplitude projection coefficients (TPAPs) associated with each radiative and non-radiative forcing of the areal averaged surface anomalies over **a** 10°S–10°N/90°–165°E, **b** 0°–10°N/90°–165°E, and **c** 10°S–0°/90°–165°E. The box with black dots over "Sum" refers to observations

is larger than that in the northern part. In addition, cloud feedback process is more important in the northern MC than in the southern MC.

5 Processes responsible for largest month-to-month surface temperature change

5.1 Warming from March to April

Strong warming occurs in the northern MC from March to April, especially over the South China Sea, and in the meantime relatively weaker warming is found in the southern MC (Figs. 2c, 6f). As the maximum solar insolation moves from the equator to the Northern Hemisphere after the spring equinox, the PTCs due to the change in solar insolation at the TOA are positive north of 5°N and negative south of 5°N (Fig. 6a). The change in surface processes warms almost the entire region except the South China Sea and a narrow band of the western tropical Pacific (Fig. 6b). As the surface processes consist of three terms including OCH, surface latent heat flux, and surface sensible heat flux, the cooling area is mainly contributed by the changes in OCH, which cools the western tropical Pacific and warms the southern MC, while the warming over the eastern MC is largely attributed to the change in surface latent heat flux, which mostly warms the entire ocean surface (figures not shown). Surface sensible heat flux contributes little to the surface temperature change during this period but shows an apparent effect of warming the land and cooling the ocean.

The patterns of PTCs due to the changes in atmospheric dynamics (Fig. 6c) and clouds (Fig. 6d) share some similarities: both warm the southern MC and cool the eastern Bay of Bengal and the western tropical Pacific. The PTCs associated with water vapor change (Fig. 6e) indicate a small cooling effect in the southern MC and a pronounced warming effect north of the equator, possibly related to the increased water vapor convergence in situ and an elevated greenhouse effect of water vapor.

5.2 Cooling from June to July

The MC region experiences its most rapid cooling from June to July and the southern MC cools more compared to the northern MC (Figs. 2f, 7f). The PTCs due to the change in solar insolation are however positive over the entire region,

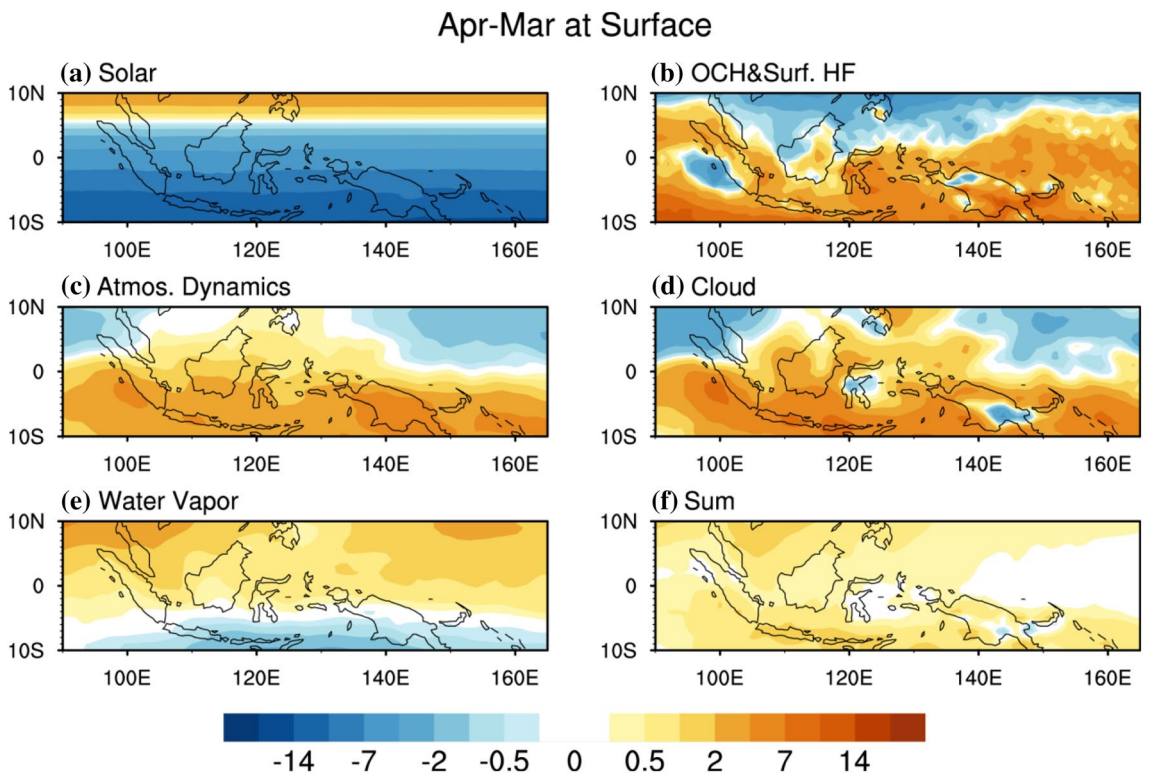

Fig. 6 Partial temperature changes (unit: K) at the surface from March to April due to changes in **a** solar insolation, **b** surface processes including OCH and surface latent/sensible heat fluxes, **c** atmospheric dynamics, **d** cloud, and **e** water vapor. **f** is the sum of all individual feedback processes

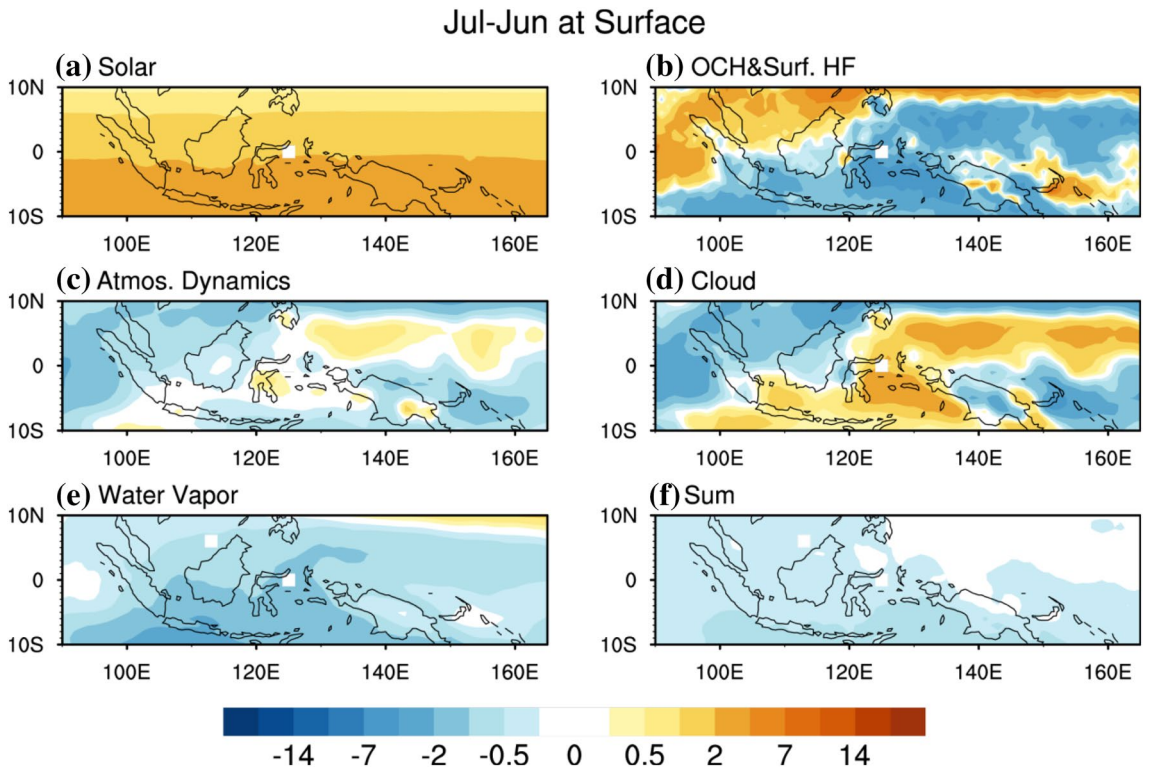

Fig. 7 Same as in Fig. 6, but for June–July

suggesting the importance of radiative and dynamical feedback processes (in comparison with the actual solar forcing) in causing the observed temperature change. For surface processes (Fig. 7b), two regions feature warm anomalies: one extending from the eastern tropical Indian Ocean to the northwestern Pacific and the other located to the east of New Guinea, mainly contributed by the variation in OCH. Also a cooling region spreads from the southern MC to the central tropical Pacific. The PTCs of surface latent heat flux are associated with the cooling in most MC and the warming in the southern MC, south of the Bay of Bengal, and the northwestern Pacific and surface sensible heat flux again shows a much smaller contribution to the temperature increment but has a similar spatial distribution compared to surface latent flux in this period, which, specifically, has a cooling effect over the land and a warming effect over the ocean, opposite to that seen in March–April (figures not shown).

The PTCs of atmospheric dynamics and cloud still share many similarities as in March–April, and the magnitude of atmospheric dynamics is smaller than that of cloud (Fig. 7c, d). The warming associated with cloud change expands from the southern MC to the western tropical Pacific and the cooling extends from the eastern Indian Ocean to the South China Sea. Water vapor turns out to be the main contributor to the June–July cooling in the southern MC (Fig. 7e), clearly a result of the anomalous moisture divergence in this region as southwesterlies and southeasterlies intrude northward during the peak period of the Asian summer monsoon.

5.3 Warming from September to October

From September to October, the southern MC warms up rapidly while small cooling occurs in the northern South China Sea, forming the second positive peak of the month-to-month temperature increment (Figs. 2i, 3b, 8f). As the maximum solar insolation moves back to the equator in September, the PTCs due to the change in solar insolation at the TOA again show positive anomalies in the southern MC and negative anomalies in the northern MC, making solar forcing one of the key contributors to the warming over the southern MC (Fig. 8a). The changes in surface processes warm the northern MC, which is contributed mainly by the OCH over the western Pacific and by surface latent heat flux over the northern MC, and cool the southern MC, which is attributed to changes in the OCH due to an increase in ocean heat content (Fig. 8b). The warming band associated with the OCH from northern Borneo to the western tropical Pacific on the other hand is largely related to changes in local energy divergence due to oceanic dynamics. Surface sensible heat flux still contributes little to the overall temperature increment (figures not shown). The warming over the southern MC also receives

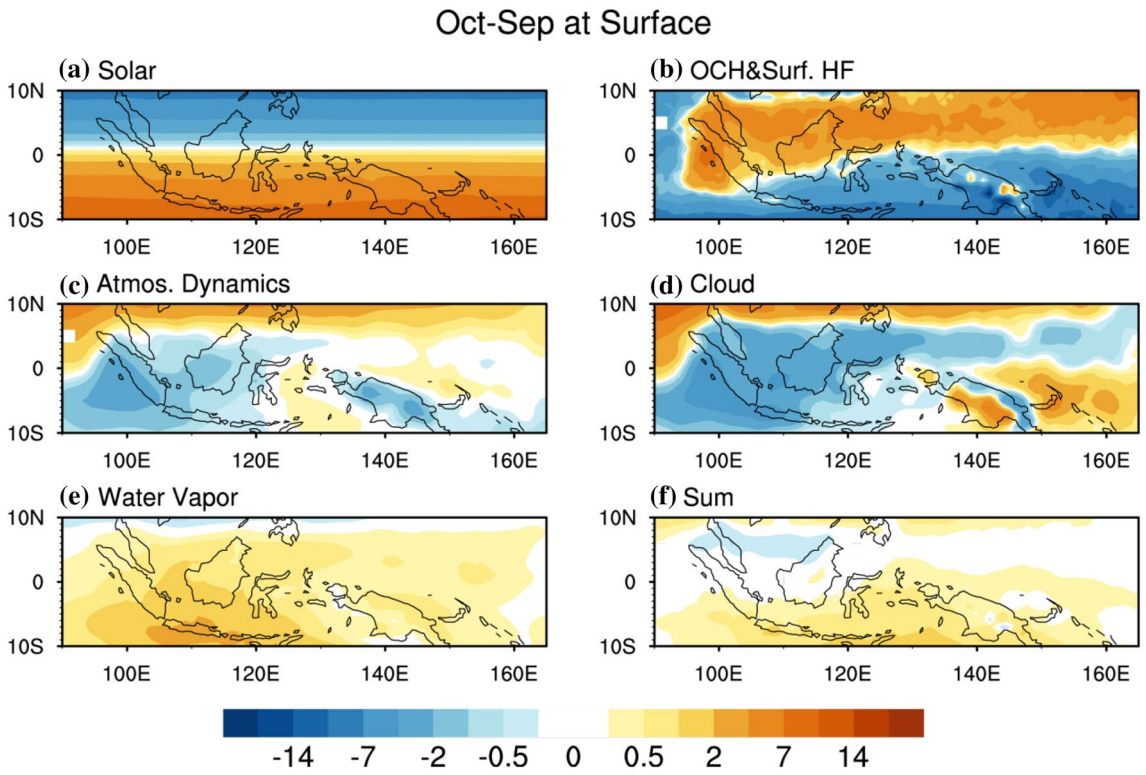

Fig. 8 Same as in Fig. 6, but for September–October

a considerable contribution from the change in water vapor (Fig. 8e). The PTCs due to changes in atmospheric dynamics are positive north of 5°N and negative in western MC (Fig. 8c). The PTCs of clouds again share a pattern similar with that of atmospheric dynamics, characterized by negative anomalies extending eastward to the western tropical Pacific and positive anomalies over New Guinea and its east (Fig. 8d).

6 Discussion

Figure 9 provides the PAPs associated with various processes for the three periods discussed above. The rapidly warming in March–April is mainly a result of the changes in radiative/dynamical feedback processes including water vapor, surface latent heat flux, clouds and atmospheric dynamics while the contributions from direct solar forcing and OCH are negative (Fig. 9a). The rapidly warming from September to October, on the other hand, is driven mainly by the changes in solar forcing (Fig. 9c). The two rapid warming months are situated right in the Asian and Australian monsoon transition seasons, as in the March–April transition from the East Asian winter monsoon to summer monsoon and in the September–October transition from the East Asian summer monsoon to winter monsoon. As shown quantitatively by the PAPs, the quick atmospheric processes (i.e., feedback processes of water vapor, clouds, and atmospheric dynamics) and ocean–atmosphere coupling (i.e., surface latent heat flux) contribute more in March–April than in September–October. Specifically, from March to April, with more solar insolation reaching the north hemisphere, there also exists a net decrease in cloudiness over the MC since the decrease south of 5°N is greater than the increase north of 5°N (Fig. 10a) and an increase in atmospheric humidity (Fig. 10d) (particularly over the northern MC) that lead to enhanced shortwave and longwave surface heating, respectively. The enhanced humidity over the northern MC results from the stronger cross-equatorial water vapor flux from the southern MC and the strengthened southwesterlies from the Bay of Bengal (Fig. 10g). Those anomalies indicate that the precipitation band quickly builds over the northern MC from March to April, and further intensifies in the boreal summer season (Fig. 10j), which reveals a sudden onset of the East Asian summer monsoon over the northern MC. However, from September to October, the contributions of atmospheric processes are relatively weaker. Clouds increase with more moist air only in the western MC (Fig. 10c, f). The enhanced convergence of water vapor flux is limited to this region while it does not extend southward as the reversal in March–April, due mainly to the limitation of

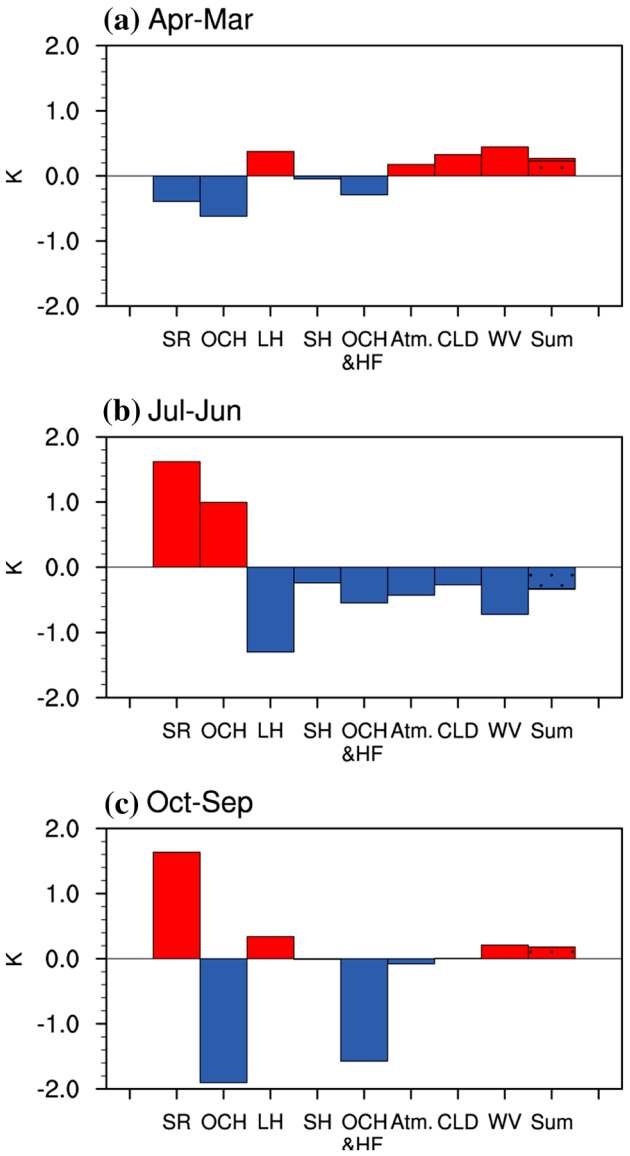

Fig. 9 PAPs at the surface over 10°S–10°N/90°–165°E due to solar insolation (SR), OCH, surface latent heat flux (LH), surface sensible heat flux (SH), surface processes (OCH and HF), atmospheric dynamic processes (Atm.), cloud (CLD), and water vapor (WV) and the sum of all feedback processes (Sum) in **a** March–April, **b** June–July, and **c** September–October. The bars with black dots overlaid on "Sum" refer to observations

enhanced northeasterly water vapor flux over the northern MC and the less strengthened cross-equatorial flux (Fig. 10i), accompanied by an anomalous deep convection over the western MC (Fig. 10l) that just moves southeastward sequentially as the East Asian winter monsoon intensifies from October to December. Thus, more contribution from quick atmospheric processes occurs in March–April coinciding with the sudden establishment of the East Asian summer monsoon over the northern MC and its adjacent regions, while the relatively less contribution from atmospheric processes in September–October is accompanied with the slowly southward moving precipitation center.

The main contributors to the rapid cooling in June–July are the same as those contributing to the rapid warming in March–April, namely changes in surface latent heat flux, water vapor, atmospheric dynamics, clouds, and surface sensible heat flux with negative contributions from direct solar forcing and OCH (Fig. 9b). Compared to change in cloudiness (Fig. 10b), the drop in atmospheric humidity over the MC clearly produces a greater cooling effect on the MC surface temperature from June to July (Fig. 10e). This drop in humidity is unambiguously tied to the northward movement of large-scale moisture convergence that occurs during the mature phase of the East Asian summer monsoon (Figs. 10e, h), with rain belts moving to East Asia and the western North Pacific (Fig. 10k).

7 Summary

In this study, based upon the energy balance in individual atmosphere–surface columns, we apply the CFRAM method to quantity the contributions of various radiative and non-radiative (dynamical) processes to the annual cycle of surface temperature of the MC. Specifically, the month-to-month temperature increments over the MC region are partitioned into PTCs associated with individual dynamical and thermodynamical processes. Overall solar forcing and surface latent flux change have the largest contributions to the surface temperature annual cycle in the MC region. The change in oceanic dynamics and heat storage often works against the month-to-month temperature change and therefore is out of phase with the annual cycle. Changes in clouds, water vapor, atmospheric dynamics and surface sensible heat flux have overall secondary but positive contributions to the annual cycle although the magnitudes of contributions vary across processes and differ over various parts of the MC region (e.g., south vs north of the equator). Therefore, in contrast to most extratropical regions where seasonal variations in the solar insolation drives the annual cycle of surface temperature, the annual cycle of the surface temperature in the MC is jointly determined by the seasonal march of the maximum solar insolation and the work of multiple atmospheric/oceanic radiative and dynamical processes.

Throughout a year, there are two positive peaks (rapid warming) in the month-to-month temperature increment, occurring in March–April and September–October, and one negative peak (rapid cooling), occurring in June–July in the MC. The rapid warming in March–April is mainly a result of the changes in water vapor, surface latent heat flux, clouds and atmospheric dynamics while the contributions from direct solar forcing and the OCH are negative. This is

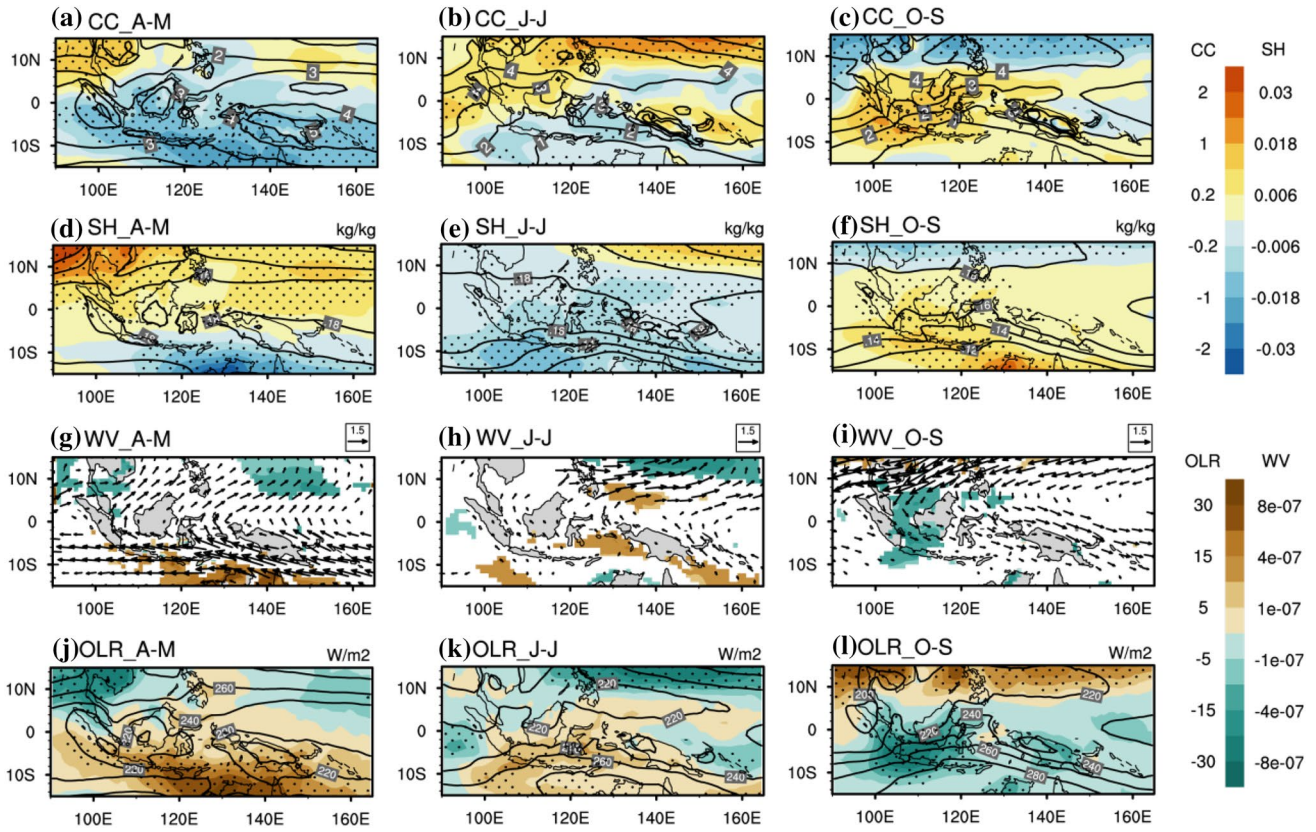

Fig. 10 Changes in **a–c** 1000–100-hPa vertically-integral cloud cover (shading, unit: 1), **d–f** 1000–400-hPa vertically-integral specific humidity (shading, unit: kg/kg), **g–i** 1000–400-hPa vertically-integral water vapor flux [vectors, unit: kg*m*hPa/(kg*s)] and its divergence [shadings, unit: kg/(kg*s)], and **j–l** outgoing long-wave radiation (shading, unit: W*m-2) in (left) March–April, (middle) June–July, and (right) September–October. Contours refer to the climatology in the former month, for example, contours in **a** represent the climatology of 1000–100-hPa vertically-integral cloud cover in March, and areas significant at the 95% confidence level are plotted with dots in **a–f** and **j–l** and shading and vectors in **g–i**

in contrast to the warming occurring in September–October, which is driven directly by the changes in solar forcing with considerable contributions from water vapor and latent heat flux change. The main contributors to the rapid cooling in June–July are the same as those for the rapid warming in March–April and the cooling also has negative contributions from direct solar forcing and OCH. As the largest contributor of the quick atmospheric processes, changes in water vapor contribute positively to the total temperature change in all three periods and they are associated with the change in the location of the center of large-scale moisture convergence during the onset and demise stages of the East Asian summer monsoon.

The contributions from individual processes differ between the two periods of rapid warming months, both of which are in the seasons of Asian and Australian monsoon transition. In this study, we provide a quantitative analysis of all radiative and non-radiative feedback processes in the two rapid warming months in monsoon transition seasons. Differences in the quick atmospheric processes and ocean–atmosphere coupling between the two periods are accompanied with temporal asymmetric movement of the deep convection belt. With almost symmetric solar insolation into the surface over MC in the two periods, more contributions from quick atmospheric processes (i.e., the feedback processes of water vapor, clouds, surface latent heat flux, and atmospheric dynamics) in March–April coexist with the sudden establishment of the East Asian summer monsoon over the northern MC and its adjacent regions, while relatively less effect by the quick atmospheric processes in September–October is with the stepwise retreat of deep convection belt. Chang et al. (2005a, b) proposed a "mass redistribution" hypothesis based on the difference in land–ocean thermal memories that the quick atmospheric processes and ocean–atmosphere coupling are linked to land–ocean distributions, which needs further investigations. The results obtained from this study allow us to look further into the asymmetric seasonal transition in precipitation by linking the surface temperature and related precipitation-driving circulation anomalies directly to individual radiative

and non-radiative processes, which will be one of the main issues to address in our future research.

Acknowledgements We appreciate the two anonymous reviewers who provided valuable comments and suggestions for improving the overall quality of this paper. The study was supported by the National Natural Science Foundation of China (Grant 41375081), the National Key Research Program of China (Grant 2014CB953904), the National Natural Science Foundation of China (Grants 41690123, 41690120, 91637208, and 41661144019), the "111-Plan" Project of China (Grant B17049), and the Jiangsu Collaborative Innovation Center for Climate Change. Yi Deng is supported by the National Science Foundation under Grants AGS-1354402 and AGS-1445956. The ERA-Interim reanalysis used in this study was provided by the European Centre for Medium-range Weather Forecasts. Calculations for this study were supported by the High-Performance Grid Computing Platform of the Sun Yat-sen University and the China National Supercomputer Center in Guangzhou. We also acknowledge the global ocean heat flux and evaporation products provided by the WHOI OA Flux project (http://oaflux.whoi.edu) funded by the NOAA Climate Observations and Monitoring (COM) program.

References

Boilley A, Wald L (2015) Comparison between meteorological reanalyses from ERA-Interim and MERRA and measurements of daily solar irradiation at surface. Renew Energy 75:135–143

Bony S et al (2006) How well do we understand and evaluate climate feedback processes? J Clim 19:3445–3482

Cai M, Lu J-H (2009) A new framework for isolating individual feedback processes in coupled general circulation climate models. Part II: method demonstrations and comparisons. Clim Dyn 32:887–900

Cai W, Rensch P, Cowan T, Hendon H (2011) Teleconnection pathways of ENSO and the IOD and the mechanisms for impacts on Australian rainfall. J Clim 24:3910–3923

Chang CP (2004) East Asian monsoon. World Scientific Publishing Co. Ptc. Ltd

Chang CP, Lau KM (1982) Short-term planetary-scale interactions over the tropics and midlatitude during northern winter. Part I: contrasts between active and inactive periods. Mon Weather Rev 110:933–946. https://doi.org/10.1175/1520-0493(1982)110,0933:STPSIO.2.0.CO;2

Chang CP, Wang Z, Ju J, Li T (2004) On the relationship between western Maritime Continent monsoon rainfall and ENSO during northern winter. J Clim 17:665–672

Chang CP, Harr PA, Chen HJ (2005a) Synoptic disturbances over the equatorial South China Sea and western Maritime Continent during boreal winter. Mon Weather Rev 133:489–503

Chang CP, Wang Z, McBride J, Liu CH (2005b) Annual cycle of Southeast Asia—Maritime Continent rainfall and the asymmetric monsoon transition. J Clim 18:287–301

Chang CP, Lu MM, Lim H (2016) Monsoon convection in the Maritime Continent: interaction of large-scale motion and complex terrain. Meteorol Monogr 56:6

Chen D, Busalacchi AJ, Rothstein LM (1994) The roles of vertical mixing, solar radiation, and wind stress in a model simulation of the sea surface temperature seasonal cycle in the tropical Pacific Ocean. J Geophys Res 99:20345–20359

Dee DP et al (2011) The ERA-Interim reanalysis: configuration and performance of the data assimilation system. Q J R Meteor Soc 137:553–597

Deng Y, Park TW, Cai M (2012) Process-based decomposition of the global surface temperature response to El Niño in boreal winter. J Atmos Sci 69:1706–1712

Deng Y, Park TW, Cai M (2013) Radiative and dynamical forcing of the surface and atmospheric temperature anomalies associated with the Northern Annular mode. J Clim 26:5124–5138

Ding Y et al (2014) Interdecadal variability of the East Asian winter monsoon and its possible links to global climate change. Chin Meteorol Soc, 90th anniversary special collection, 28:693–713

Fu Q, Liou KN (1992) On the correlated K-distribution method for radiative transfer in nonhomogeneous atmosphere. J Atmos Sci 49:2139–2156

Fu Q, Liou KN (1993) Parameterization of the radiative properties of cirrus clouds. J Atmos Sci 50:2008–2025

Hendon HH (2003) Indonesian rainfall variability: impacts of ENSO and local air-sea interaction. J Clim 16:1775–1790

Hu XM, Yang S, Cai M (2016) Contrasting the eastern Pacific El Niño and the central Pacific El Niño: Process-based feedback attribution. Clim Dyn 47:2413. https://doi.org/10.1007/s00382-015-2971-9

Hung CW, Yanai M (2004) Factors contributing to the onset of the Australian summer monsoon. Q J R Meteorol Soc 130:739–761

Hung CW, Liu X, Yanai M (2004) Symmetry and asymmetry of the Asian and Australian summer monsoons. J Clim 17:2413–2426

Kodera K, Kuroda Y (2002) Dynamical response to the solar cycle. J Geophys Res 107:ACL 5-1–ACL 5-12. https://doi.org/10.1029/2002JD002224

Lau KM, Chan PH (1983) Short-term climate variability and atmospheric teleconnections from satellite-observed outgoing longwave radiation. Part II: lagged correlations. J Atmos Sci 40:2751–2767

Lau KM, Chang CP (1987) Planetary scale aspects of winter monsoonand teleconnections. In: Chang C-P, Krishnamurti TN (eds) Monsoon meteorology. Oxford University Press, Oxford, pp 161–202

Li Y, Yang S (2010) A dynamical index for the east Asian winter monsoon. J Clim 23(15):4255–4262

Li Y, Yang S (2017) Feedback attributions to the dominant modes of East Asian winter monsoon variations. J Clim 30:905–920

Lu JH, Cai M (2009a) Quantifying contributions to polar warming amplification in an idealized coupled general circulation model. Clim Dyn 34:669–687

Lu JH, Cai M (2009b) A new framework for isolating individual feedback process in coupled general circulation climate models. Part I: formulation. Clim Dyn 32:873–885

Matsumoto J (1992) The seasonal changes in Asian and Australian monsoon regions. J Meteorol Soc Jpn 70:257–273

McBride JL, Haylock MR, Nicholls N (2003) Relationships between the Maritime Continent heat source and the El Niño-Southern Oscillation phenomenon. J Clim 16:2906–2914

Meehl GA (1987) The annual cycle and interannual variability in the Tropical Pacific and Indian Ocean regions. Mon Weather Rev 115:27–50

Neale R, Slingo J (2003) The Maritime Continent and its role in the global climate: a GCM study. J Clim 16:834–848

Nicholls N, Lavery B, Frederiksen C, Drosdowsky W, Torok S (1996) Recent apparent changes in relationships between the El Niño-Southern Oscillation and Australian rainfall and temperature. Geophys Res Lett 23:3357–3360

Park T-W, Deng Y, Cai M (2012) Feedback attribution of the El Niño—Southern Oscillation—related atmospheric and surface temperature anomalies. J Geophys Res 117:D23101. https://doi.org/10.1029/2012JD018468

Philander SGH (1985) El Niño and La Niña. J Atmos Sci 42:2652–2662

Qian J (2008) Why precipitation is mostly concentrated over islands in the Maritime Continent. J Atmos Sci 65:1428–1441

Ramage CS (1968) Role of a tropical "Maritime Continent" in the atmospheric circulation. Mon Weather Rev 96:365–370

Ramage CS (1971) Monsoon meteorology. Academic Press, New York, p 296

Schmidt FH, Ferguson JHA (1951) Rainfall types based on wet and dry period ratios for Indonesia with western New Guinea, vol 42. Verhandelingen, pp 77 **(plus figures)**

Sejas SA, Cai M, Hu A, Meehl GA, Washington W, Taylor PC (2014) Individual feedback contributions to the seasonality of surface warming. J Clim 27:5653–5669

Simpson J, Keenan TD, Ferrier B, Simpson RH, Holland GJ (1993) Cumulus merger in the Maritime Continent region. Meteorol Atmos Phys 51:73–99

Smith SD (1988) Coefficients for sea surface wind stress, heat flux, and wind profiles as a function of wind speed and temperature. J Geophys Res 93:15467–15472

Sui CH, Lau KM (1992) Multiscale phenomena in the tropical atmosphere over the western Pacific. Mon Weather Rev 120:407–430

Sukanto M (1969) Climate of Indonesia. Climates of Northern and Eastern Asia. In: Arakawa H (ed) World survey of climatology, vol 8, Elsevier, pp 215–229

Trenberth KE, Guillemot CJ (1996) Physical processes involved in the 1988 drought and 1993 floods in North America. J Clim 9:1288–1298

Uppala SM, Dee D, Kobayashi S, Berrisford P, Simmons A (2008) Towards a climate data-assimilation system: status update of ERA-Interim. ECMWF Newslett 115:12–18

van den Dool HM, Saha S (1993) Seasonal redistribution and conservation of atmospheric mass in a general circulation model. J Clim 6(1):22–30

Wang B, Wu Z, Chang CP, Liu J, Li J, Zhou T (2010) Another look at interannual-to-interdecadal variations of the East Asian winter monsoon: the northern and southern temperature modes. J Clim 23:1495–1512

Webster PJ, Yang S (1992) Monsoon and ENSO: selectively interactive systems. Q J R Meteorol Soc 118:877–926

Wu B, Zhou T, Li T (2009) Contrast of rainfall-SST relationships in the western North Pacific between the ENSO-developing and ENSO-decaying summers. J Clim 22:4398–405

Yanai M, Tomita T (1998) Seasonal and interannual variability of atmospheric heat sources and moisture sinks as determined from NCEP–NCAR reanalysis. J Clim 11:463–482

Yang S, Lau KM, Kim KM (2002) Variations of the east Asian jet stream and Asian–Pacific–American winter climate anomalies. J Clim 15:306–325

Zhu B, Wang B (1993) The 30–60 days convection seesaw between the tropical Indian and western Pacific Oceans. J Atmos Sci 50:184–199